A Study on the Wave Dispersion in Concrete Due to Damage; Numerical Observations and Theoretical Predictions

Georgios Livitsanos[1], Abdul Bashit Ahmadi[1], Dimitrios G. Aggelis[1], Theodore V. Gortsas[2], and Demosthenes Polyzos[2(✉)]

[1] Department of Mechanics of Materials and Constructions, Vrije Universiteit Brussel, Brussels, Belgium
[2] Department of Mechanical Engineering and Aeronautics, University of Patras, Patras, Greece
polyzos@upatras.gr

Abstract. Experimental results have shown that waves propagating in non-homogeneous and composite materials exhibit dispersive behavior even in cases where they are characterized by isotropic effective properties. Concrete is such a material and at both its fresh and hardened state wave dispersion is observed. The dispersion becomes more pronounced when microdefects like microcracks and air voids appear in the main body of the concrete. The goal of the present work is threefold: first to examine numerically the contribution of various defects to the wave dispersion in concrete, second to show through numerical experiments that circular voids embedded in a concrete matrix is a good approximation for simulating wave dispersion in damaged concrete and third to capture the dispersive behavior of a longitudinal plane wave propagating in damaged concrete with the aid of two theories, namely the multiple wave scattering model of Waterman and Truell and the generalized elastic theory of a strain gradient elastic material. Numerical, experimental and theoretical results are compared and discussed throughout the paper.

1 Introduction

Ultrasonic pulse velocity is a widely spread non-destructive testing parameter that has proven very reliable and relatively easy to use for decades. The empirical correlations with strength of materials (especially concrete), although not theoretically justified, seriously contribute in the evaluation of structural condition [1]. In the domain of cementitious media the wave velocity is used as the first demonstrator of the structural health and allows strength prediction either in hardening or hardened concrete [2]. The majority of the scientific articles and even more of the in-situ cases, employ ultrasonic pulse velocity as the main parameter for characterization. The reason is the relative easiness to apply and the reliability on the strength estimation. Commercial, high-voltage ultrasonic systems employ transducers of a fixed frequency (usually 54 kHz) and detect the onset of the waveform at the receiving transducer through its first crossing above a fixed threshold. Many correlations have seen publicity showing that pulse velocities above 4000 m/s are measured in good quality concrete while velocities

T. Triantafyllidis (Ed.): *Recent Developments of Soil Mechanics and Geotechnics in Theory and Practice*, LNACM 91, pp. 183–198, 2020.
https://doi.org/10.1007/978-3-030-28516-6_10

below 3000 m/s indicate problematic state. Relatively recently, the influence of frequency has been studied. It is shown that as the heterogeneity of the medium increases, the dependence of velocity on frequency (dispersion) becomes stronger. The heterogeneity in concrete is related to the impedance mismatch between its constituents. This has been theoretically treated using scattering models and more recently with gradient elastic theories [3–5]. To a limited extent, a mismatch is noted between the cement matrix and the stiffer aggregates although in general, their density discrepancies are not strong. More intensive scattering or microstructural effects are expected by air bubbles (entrapped or entrained air) and cracks, as in these cases the impedance mismatch is huge and the inclusions are in essence voids. The easier way to model these heterogeneities is the spherical shape. This is supposed to result in a wave velocity and overall behavior, in general, close to a case with random inclusions and of random distribution, provided of course that the volume content and the mechanical properties are constant. Though this perception is common in the field of wave scattering, there is no concrete study in the international literature to prove this for a variety of shapes of inclusions. In this paper, numerical simulations are conducted using several shapes of voids (inclusions with properties of air), distribution patterns and volume contents. The results allow for comparison between the shapes, showing that even with the same content, the inclusion shapes are responsible even for 20% difference in UPV. Thus, one aim of the study concerns the basic level of wave propagation and is conducted through numerical simulations, a second aim is the comparison with experimental data from cementitious mortar with different volume content of polystyrene inclusions, while a third aim is to verify the observed wave dispersion via the multiple wave scattering model of Waterman and Truell [6] and the use of the simple strain gradient elastic theory of Mindlin [7].

2 Numerical Simulation Model

In this section, a numerical experiment dealing with the propagation of a plane longitudinal elastic wave in a concrete specimen containing air voids in different shapes and orientation is carried out. For the shake of simplicity plane strain conditions are considered. The cases examined were solved numerically in order to produce the waveform of the receiver and extract the transit time of the onset of the wave. The fundamental equation governing the two-dimensional propagation of elastic waves in an elastic medium, ignoring viscous losses, is as follows:

$$\mu\nabla^2\mathbf{u} + (\lambda + \mu)\nabla\nabla\cdot\mathbf{u} = \rho\frac{\partial^2\mathbf{u}}{\partial t^2} \tag{1}$$

where $\mathbf{u} = \mathbf{u}(x, y, t)$ is the time-varying displacement vector, ρ is the material density, λ and μ are the first and second Lamé constants, respectively, and t is time. The simulations were conducted with commercially available software wave2000 [8], which solves the above equation using the finite difference method in the plane strain case. Equation (1) is solved at discrete points with respect to the boundary conditions of the model, which include the input source that has predefined time-dependent displacements at a given

location and a set of initial conditions [9]. For heterogeneous geometries like the ones studied herein, wave propagation in each distinct homogeneous phase is solved according to Eq. (1), while the continuity conditions for stresses and strains must be satisfied on the interfaces [9].

The mechanical properties of the different materials are shown in Table 1. In total three different types of materials were considered: cementitious matrix, voids (inclusions of air), and aggregates.

Table 1. Material properties used for the numerical model.

Material	Density ρ (kg/m^3)	First Lame λ (GPa)	Second Lame μ (GPa)	Ultrasonic velocity, C (m/s)
Cement matrix	2400	11.1	16.7	4216
Air	1.2	0.0001	0.00001	316

The basic geometry was a square of 100 mm side on which the different inhomogeneities were incorporated, as shown in Fig. 1. Infinite boundary conditions were applied to all sides of the geometry. The "pulser" was triggered by a displacement excitation of 10 cycles of constant amplitude and the simulation was repeated for several frequencies, namely 50 kHz, 150 kHz, 300 kHz and 500 kHz in order to estimate the effect of the different wavelengths (roughly from 80 mm down to 8 mm). The "receiver" was placed on opposite side of the geometry allowing for a propagation distance of 100 mm between pulser and receiver. One example of a geometric model of a matrix with few circular air inclusions is shown in Fig. 1.

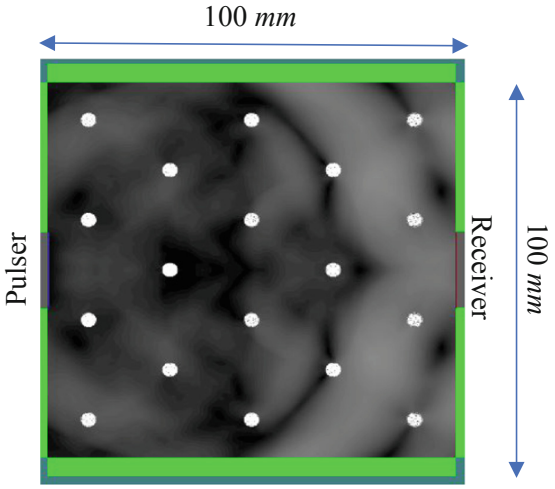

Fig. 1. Geometrical model for the numerical simulations.

The "receivers" provide the average vertical displacement over their length, meaning that the receiver signal represents the average response over a number of nodes. The simulation accuracy depends on the density of the points on which the equation of motion is solved. Thus, preliminary simulations were conducted on a specific geometry (with circular inclusions) to estimate the effect of mesh size on accuracy as well as computation time. Mesh sizes from 8 mm down to 0.8 mm were selected. It is seen that the resulted velocity is certainly influenced by the selected resolution showing however convergence at 1 mm (Fig. 2). Therefore, the analysis was done with the resolution of 1 mm, which was just 0.0066% different than the finest resolution tried, but considerably faster. This resolution is much lower than the shortest applied wavelength of 8 mm corresponding to the highest frequency applied of 500 kHz. The time resolution is 0.01537 μs, corresponding to sampling rate of 65 MHz, well above the applied frequencies.

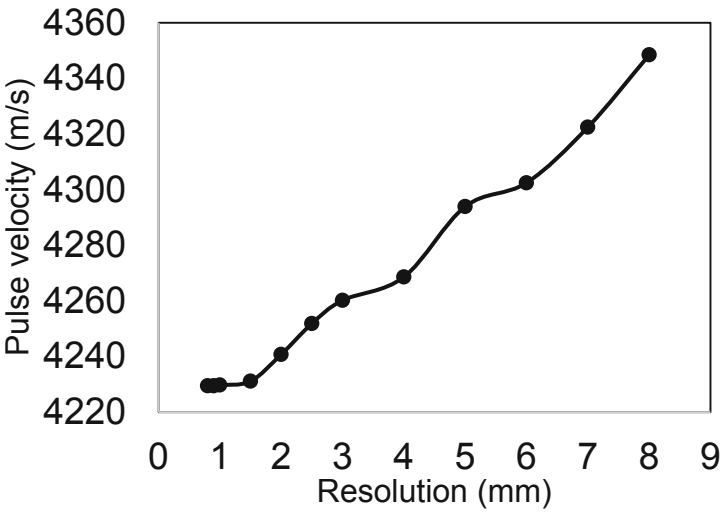

Fig. 2. Convergence of pulse velocity results for finer resolution (mesh size).

Three different contents of inclusions were used, namely 2%, 5% and 10%. In addition, several shapes of inclusions were applied. In total ten different cases of single shaped voids (and orientations when applicable) were applied, and Fig. 3 shows five indicative cases, concerning circles, squares, ellipses, rectangular at different orientation. For the two latter, four different orientations of the longitudinal axis of the inclusion were applied (horizontal, vertical and $\pm 45^{o}$). The dimensions of the different inclusion shapes are shown in Table 2. The common characteristic for all shapes is their area which is fixed to 11.11 mm^2.

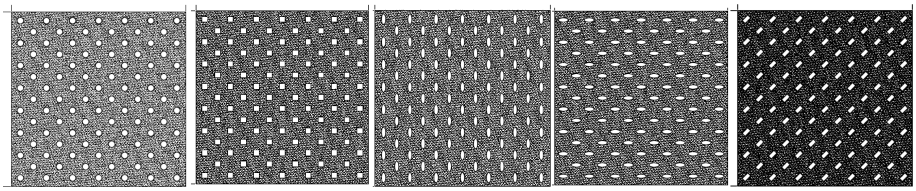

Fig. 3. Indicative patterns of inclusions in the model (from left to right: circular, square, vertical ellipses, horizontal ellipses, diagonal rectangles).

Table 2. Basic shapes and dimensions of inclusions

Circle	radius 1.9 mm
Rectangle	4.54x2.45 mm
Oval	2.9x1.2 mm
Square	side 3.33 mm

Apart from the single shape of inclusions, five different patterns were created by mixing the different shapes. Three of them are shown in Fig. 4a. Finally, two cases with random patterns of circular voids were created as shown in Fig. 4b, making a total of 16 different cases.

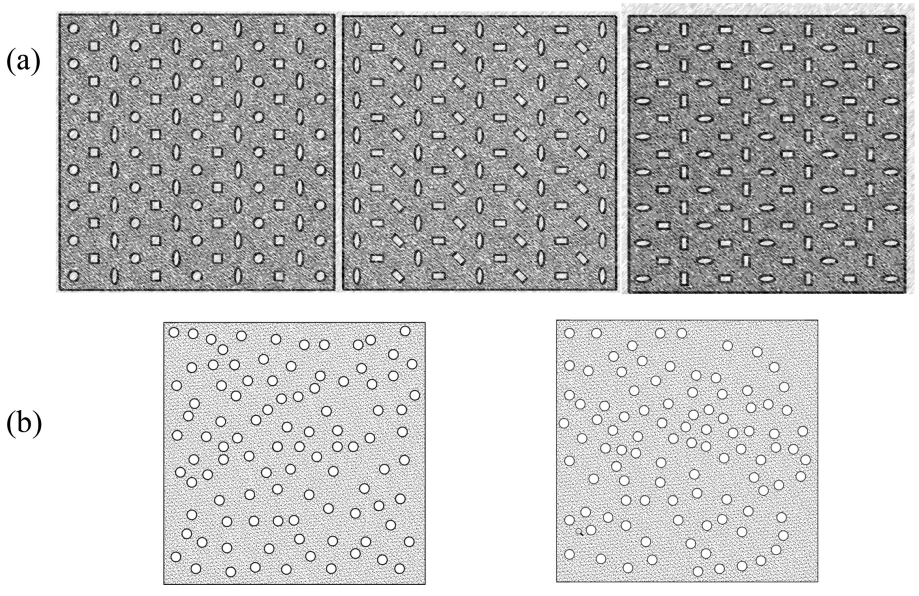

Fig. 4. (a) Indicative patterns of mixed inclusions, (b) random pattern of spherical inclusions.

3 Results

The transit time used for velocity calculations was determined by the first disturbance on the receiver's waveform (no threshold needed as all previous waveforms points were zero). Two indicative waveforms are shown in Fig. 5 concerning the response to 150 kHz for the pure matrix and the matrix with circular inclusions to the content of 10%. The effect of heterogeneity is seen both in the delayed onset and the amplitude of the waveform of 10% compared to 0%.

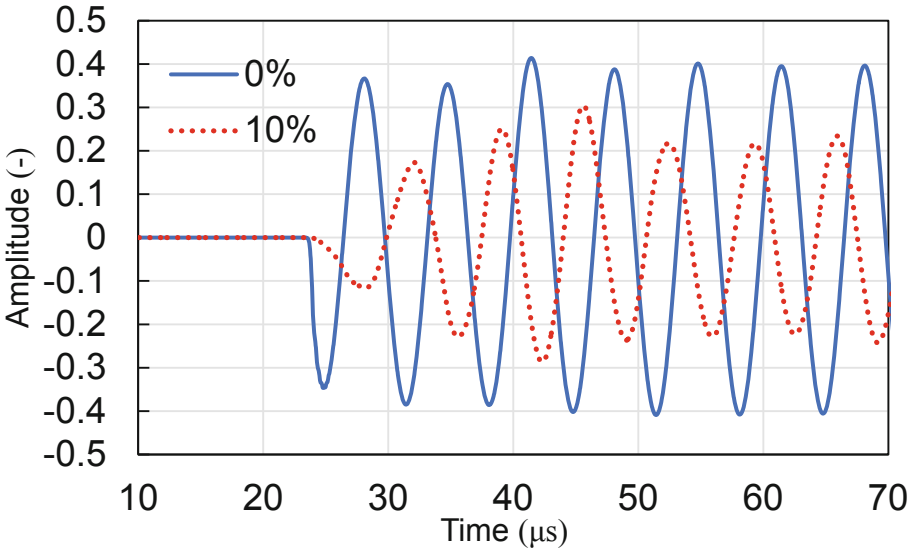

Fig. 5. Simulated waveforms for 150 kHz excited frequency for matrix with 0% and 10% of circular inclusions.

Figure 6 shows the pulse velocity vs. frequency curves for some indicative heterogeneity patterns with 10% content. In all cases the velocity increases towards the 500 kHz, something that as will be seen later is also in agreement with the solution of the scattering model of Waterman and Truell [6]. Nevertheless, similar results have been reported for the field of concrete, suggesting increase of wave velocity with increase of frequency for sound and damaged material [3, 10]. The cases with the least dispersion are the ones with the horizontal inclusions (ellipses and rectangles). The strongest dispersion along with the lower velocity curves are shown by the vertical orientation of the same shapes. The diagonal orientation shows an intermediate velocity curve. The circle shape of inclusions comes very close to the square shape starting at 3986 m/s and reaching 4210 m/s for 500 kHz. It is evident that as the frequency increases, the discrepancies between the different shapes becomes negligible except for the extreme cases of vertical inclusions which exhibit the strongest reflection fronts against the propagating wave. Excluding these two extreme cases, the circular shape seems to be a good approximation yielding velocities in the average of the other cases.

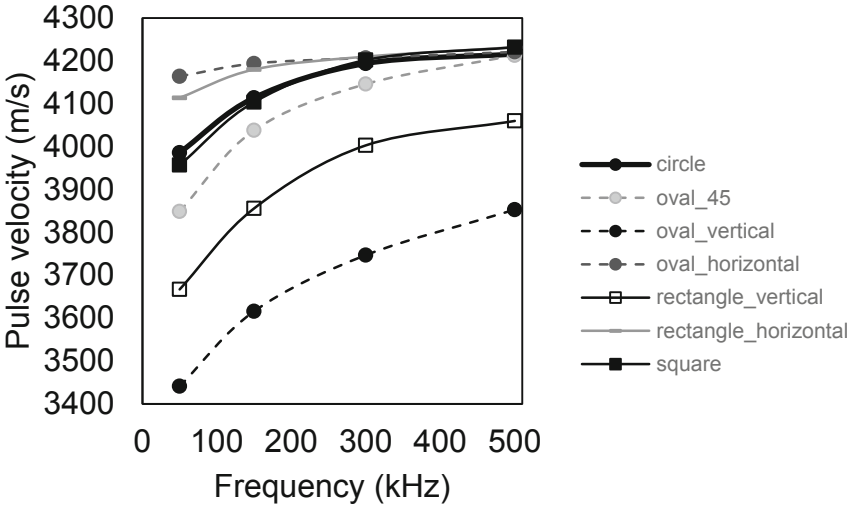

Fig. 6. Pulse velocity vs. frequency curves for different inclusion shapes and patterns of content 10%.

Figure 7 shows the corresponding results for the mixed shapes cases, including again the circular inclusion shape for comparison. The basic trend of the increasing velocity with frequency holds for all cases and while there are patterns exhibiting higher or lower velocity curve than the circular shape, the latter's curve is placed closer to the top rather than the bottom curve, something also noted earlier in Fig. 6.

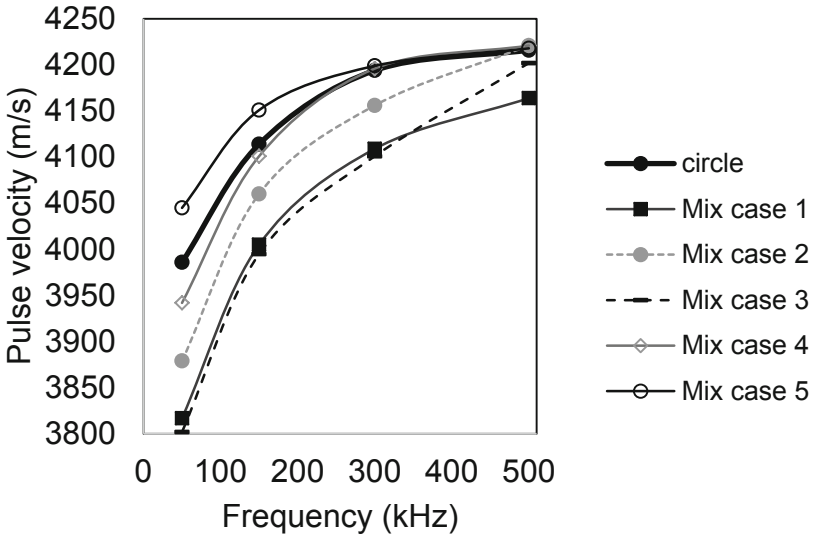

Fig. 7. Pulse velocity vs. frequency curves for different mixed shape patterns of content 10%.

The following graph (Fig. 8) concerns circular inclusions but with three different distribution patterns. One is the rectangular pattern shown in Fig. 3 (left), while the other two are random and shown in Fig. 4b. The curves are close with maximum deviation of 50 m/s (approximately 1.25%) at 50 kHz. The distribution pattern seems therefore, not to crucially influence the result provided that the inclusion shape and content are constant.

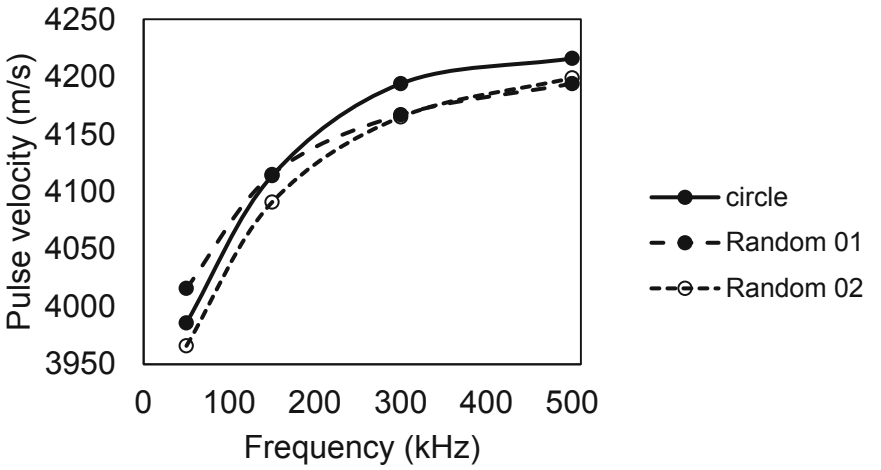

Fig. 8. Pulse velocity vs. frequency curves for circular inclusions and different patterns of content 10%.

In order to have a clear comparison for different shapes and combinations of them, Fig. 9 includes the pulse velocity values at 50 kHz for 10% content. All the applied patterns are shown for completeness. What is again evident is that apart from the cases of ellipsoidal and rectangular horizontal inclusions which do not pose strong obstruction to wave propagation and thus result in higher velocities, the circular case of scatterer (either in specific distribution pattern or random) presents velocities at the high level of 4000 m/s, only 5% less than the pure matrix velocity of 4216 m/s. Other inclusion shapes/orientations present lower velocities like the ellipsoidal at 45^{o} to the propagation direction, which is close to 3850 m/s, while long inclusions with their axis perpendicular to the propagation direction drop to values close to 3400 m/s. The circular case presents the 5th highest pulse velocity from the presented 16 cases.

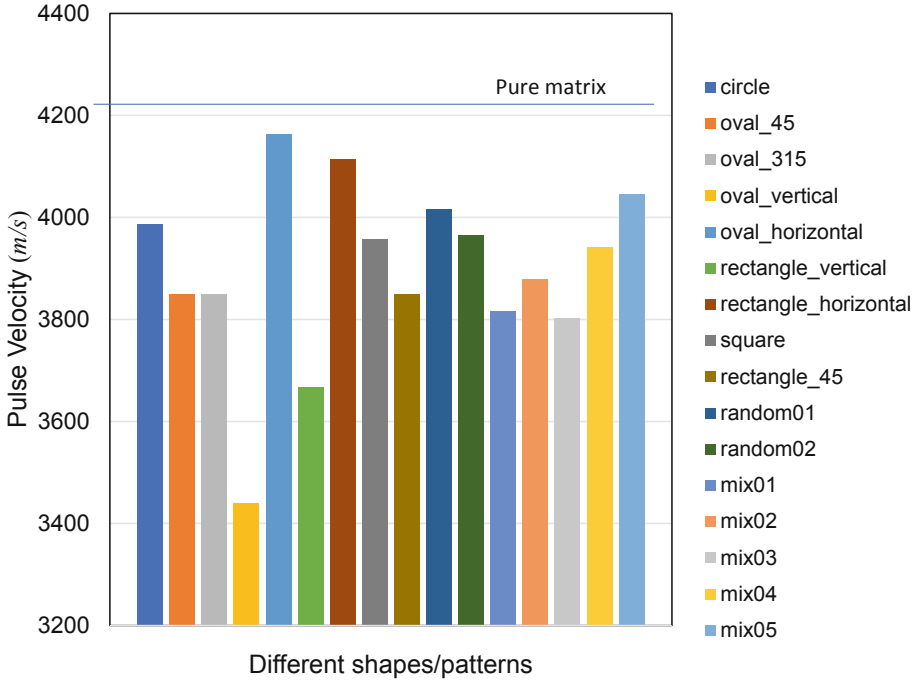

Fig. 9. Pulse velocities for 50 kHz for all cases of inclusion shapes and geometrical distribution patterns for content of 10%.

4 Comparison with Experimental Data

The above numerical results are compared with experimental results on the effect of frequency on pulse velocity. The experimental data are taken from [11], where film-shape light inclusions of 15 × 15 × 0.5 mm were added during mixing of cementitious mortar in volume contents from 0% (reference), 1%, 5% to 10%. Figure 10a shows the experimental pulse velocity vs. frequency curves. All curves (even plain mortar) exhibit a dispersive trend, which is expected due to the inherent heterogeneity of mortar. This dispersion is more pronounced for higher number of voids leading to quite strong discrepancies between the velocity at 30 kHz (3390 m/s) and the velocity of 500 kHz (3900 m/s) for 10% vol. content. The corresponding numerical results are shown in Fig. 10b. There, the curves corresponding to the ellipsoidal vertical shape are presented revealing many similarities to the experimental results. The frequency dependence increases for high amount of voids, while even the values are quite close. Obviously the wave dispersion observed in Fig. 10a is due not only to the presence of the randomly oriented film-shape light inclusions but also to the heterogeneity of the cementitious mortar matrix. Since all numerical experiments consider non-dispersive matrix, it is expected that the mixed models of Fig. 4a provide wave behavior being less dispersive than that observed experimentally. This explains why in Fig. 10(b) the numerical results are close to experimental ones, when vertical ellipsoidal voids are

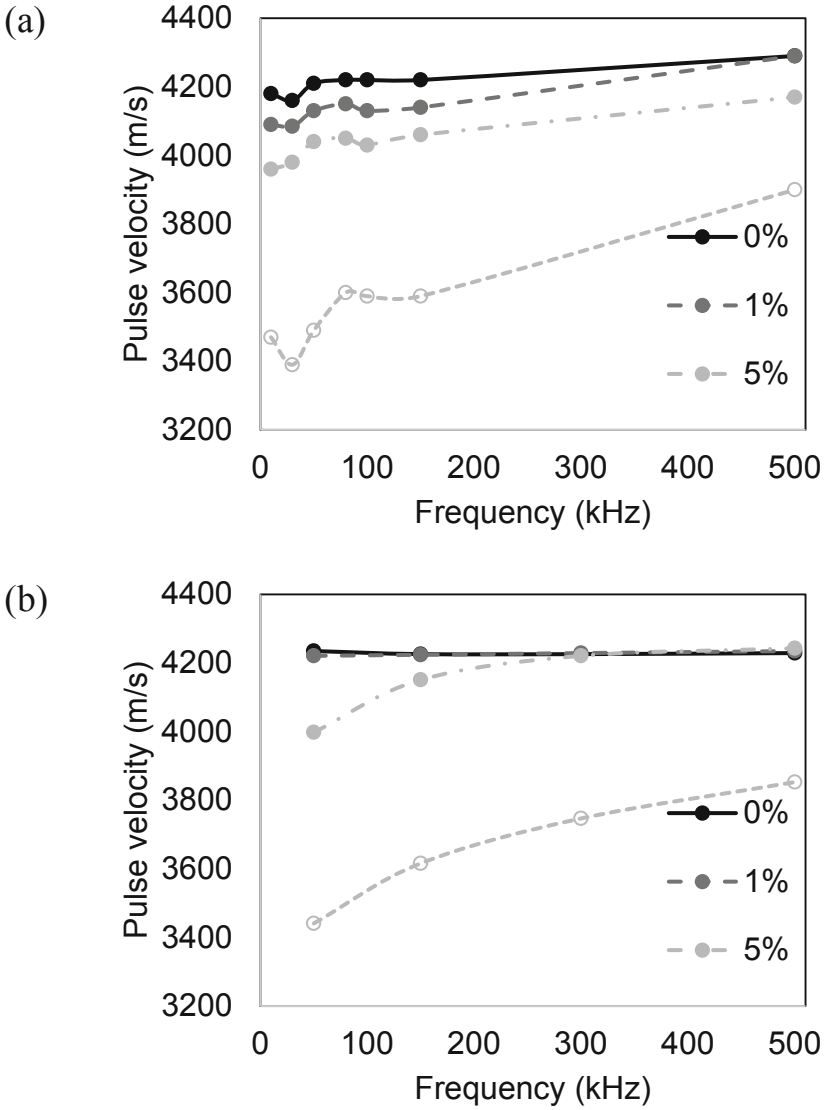

Fig. 10. (a) Experimental pulse velocity vs. frequency curve for concrete with different percentage of light plate inclusions [10]. (b) Numerical pulse velocity vs. frequency curve for ellipsoidal voids vertical to propagation.

considered. Indicatively for the 10% voids case, the velocity at low frequencies for both numerical and experimental approach is at the level of 3400 m/s, while for the highest frequency it reaches 3800–3900 m/s. In addition, it is interesting to note that the discrepancy between 10% and 5% is much more than between 5% and 0% both in numerical and experimental, showing the accumulated effect of damage.

5 Theoretical Predictions

The main purpose of this section is to develop an understanding of the mechanism responsible for the dispersive behavior of the longitudinal elastic waves observed numerically and experimentally in Sects. 3 and 4, respectively. Depending on the frequency, all the results obtained so far converge to the conclusion that voids of various shapes affect drastically, even in very small volume concentrations, the velocity of propagating waves. Many researchers have proposed the multiple scattering of the incident wave by the distributed voids as the main mechanism of the observed wave dispersion [3, 12–14]. Others believe that the microstructure of the nonhomogeneous material is responsible for the phenomenon. However, due to the lack of internal length scale parameters that correlate the microstructure with the macrostructure, the classical theory of elasticity is not able to capture wave dispersion in those materials. For this reason enhanced elastic theories like the micropolar and stainn gradient elasticity are preferred [5, 15–17]. In this section the scattering theory of Waterman and Truell [6] and the strain gradient elastic theory of Mindlin [7] are employed in order to explain the numerical results presented in Sect. 3. For demonstration purpose, only circular voids are considered.

5.1 Wave Dispersion Predictions via the Waterman and Truell Scattering Model

According to Waterman and Truell [6], the wave dispersion of an elastic wave propagating in a nonhomogeneous elastic medium is undertaken through the multiple scattering theory which, solves problems dealing with the scattering of incident plane waves by a cloud of inclusions embedded in an elastic matrix. According to this theory, the wave dispersion and attenuation in a nonhomogeneous medium can be obtained in terms of the particle/void concentration and the forward as well as the backward far field scattering amplitudes. More precisely, the wave dispersion and attenuation is represented via the frequency-dependent complex wavenumber, $k(\omega)$, which is expressed in terms of the void concentration and the forward as well as the backward far-field scattering amplitudes, i.e.

$$\left(\frac{k(\omega)}{k_c}\right)^2 = 1 + \frac{3\varphi}{k_c^2 R^3} f(0) + \frac{9\varphi^2}{4k_c^4 R^6}\left[f^2(0) - f^2(\pi)\right] \tag{2}$$

where k_c is the real wavenumber of the matrix material, φ the volume fraction of the inclusion, R the particle radius when spherical particles are considered and $f(0)$ and $f(\pi)$ are the complex single scattering forward and backward scattering amplitudes, respectively. The latter are evaluated analytically for circular voids [18] and numerically for arbitrarily shaped cavities.

It should be noticed here that the Waterman and Truell theory ignores the interaction between the inclusions and for this reason its applicability is confined to concentrations of particles or voids being below to 12%. For higher concentrations can be replaced by the iterative effective medium approximation technique illustrated in [19].

For the concrete matrix perforated by 10% of circular voids, described in Sect. 2, the phase velocity of a longitudinal plane wave is evaluated according to (2) and depicted as a function of frequency in Fig. 11. The results are compared to corresponding numerical ones obtained by the wave2000 commercial code [8] as it is explained in Sect. 3. As it is apparent, relation (2) provides a reasonable explanation for the wave dispersion occurred in the concrete due to the presence of 10% circular cavities.

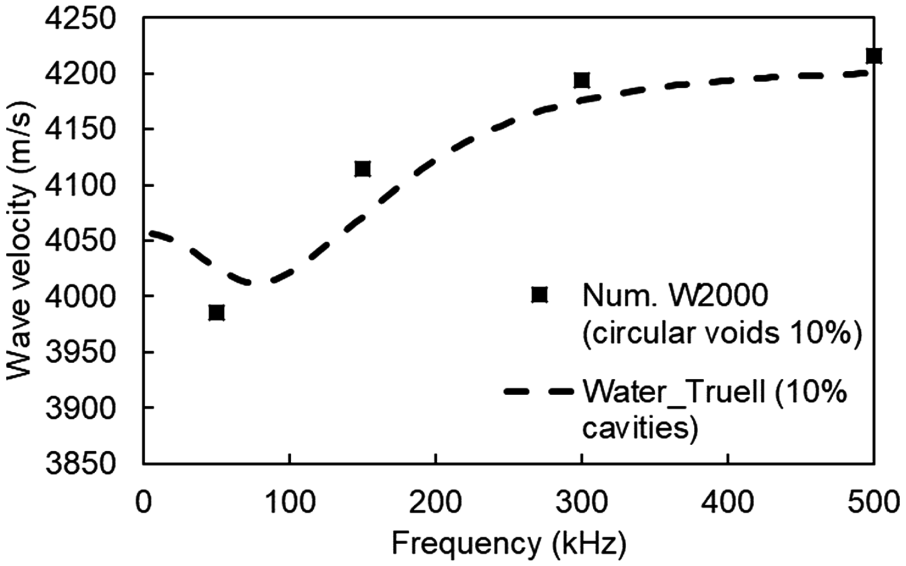

Fig. 11. Phase velocity vs. frequency curve for 10% vol. assuming circular shape of inclusions, based on the scattering model of Waterman and Truell [6].

5.2 The Concrete as a Strain Gradient Elastic Material

Mindlin [7], in the Form-II version of his strain gradient elastic theory, considered that the potential energy density is a quadratic form not only of the strains but also of the gradient of strains. Similarly, the kinetic energy appears to be a quadratic function of both velocity and gradient of velocity. Under those consideration, his theory concludes to an equation of motion, which in its simplest form, can be written as

$$(1 - g^2\nabla^2)[\mu\nabla^2\mathbf{u} + (\lambda + \mu)\nabla\nabla \cdot \mathbf{u}] = \rho(\ddot{\mathbf{u}} - h^2\nabla^2\ddot{\mathbf{u}}) \tag{3}$$

where $\mathbf{u}$ stands for the displacement vector, λ, μ represent the classical elastic Lame constants, ∇ and ∇^2 indicate the gradient and Laplace operator, respectively, dots indicate differentiation with respect to time and g, h are the stiffness and inertia, respectively, internal length scale parameters that correlate the microstructure with the dynamic macrostructural behavior of the strain gradient elastic material.

Considering displacements as harmonic plane waves of frequency ω, Eq. (3) leads to the following dispersion relation

$$V_{p,s} = \frac{\omega}{k_{p,s}} = C_{p,s}\sqrt{\frac{1+g^2k_{p,s}^2}{1+h^2k_{p,s}^2}} \tag{4}$$

where $V_{p,s}$ represents the phase velocity of a longitudinal (p) or transverse (s) plane wave propagating in the strain gradient elastic material, while $C_{p,s}$ and $k_{p,s}$ stand for the phase velocity and the wave number, respectively, of a plane wave traveling in a classical linear elastic medium characterized by the Lame constants λ, μ.

Equation (4) reveals that, unlike the classical elastic case characterized by constant velocities of longitudinal and shear waves and hence nondispersive wave propagation, the gradient elastic is characterized by phase velocities for longitudinal and shear waves, which are functions of the wave number, indicating wave dispersion. This dispersion is imposed with the presence of the two intrinsic parameters g^2 and h^2. It is apparent that for $g = h = 0$, Eq. (4) reads $V_{p,s} = C_{p,s}$, but what is interesting here is that dispersion disappears when the micro-stiffness coefficient g is equal to micro-inertia one h. Dispersion relation (4) can be written in terms of frequency as follows:

$$V_{p,s} = C_{p,s}\frac{1-\left(\frac{\omega h}{C_{p,s}}\right)^2+\sqrt{\left(1-\left(\frac{\omega h}{C_{p,s}}\right)^2\right)^2+\left(2\frac{\omega g}{C_{p,s}}\right)^2}}{2} \tag{5}$$

Considering the material of the previous subsection as a homogenized strain gradient elastic medium and utilizing the dispersion relation (5), the frequency dependent phase velocity of a longitudinal plane wave propagating in the considered strain gradient elastic material is evaluated and depicted in Fig. 12.

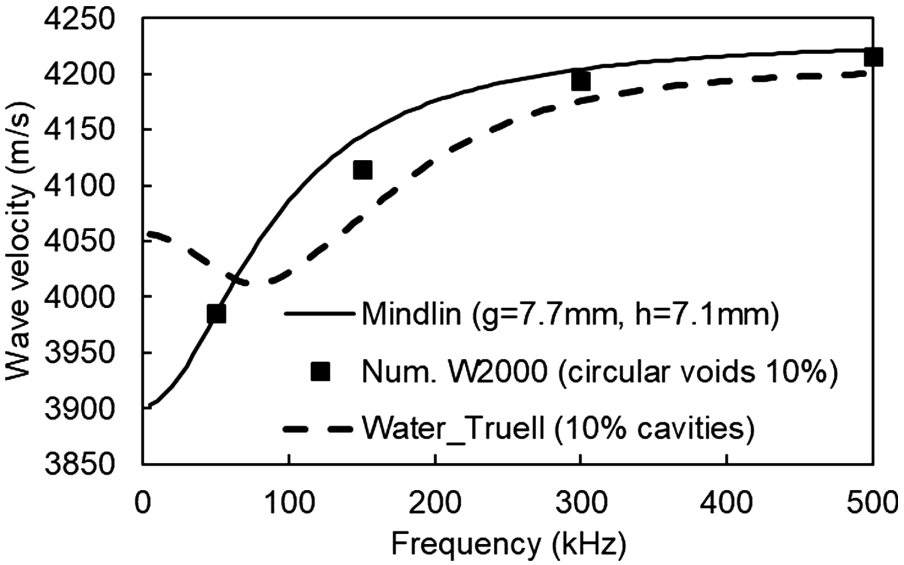

Fig. 12. Wave velocity vs. frequency according to Mindlin's gradient elastic theory [7]

It is obvious that both Waterman and Truell and strain gradient elastic approaches exhibit a similar trend with increasing velocity for higher frequency up to 500 kHz while some differences only exist at the low band of frequency below 50 kHz. The values of the Mindlin's microstructural coefficients leading to a good agreement with numerical results are g (micro-stiffness) = 7.7 mm and h (micro-inertia) = 7.1 mm. It is noted that the circular void (the case of which is included in the comparison of Fig. 12) has a diameter of 3.8, being approximately the half of the value of microstiffness.

Due to the interaction of a propagating elastic wave with the voids of the concrete material, the choice of the Waterman and Truell multiple scattering model as a candidate theory to explain the observed wave dispersion was quite reasonable. The spontaneous question here is why to consider one the concrete with the circular voids as a strain gradient elastic material. It is well known that the strain gradient elasticity is a theory, which by definition can be applied only in materials where significant strain gradients occur. Thus, in order to give an answer to that question, the traction field that follows the direction of a propagating harmonic longitudinal wave is evaluated for the cases of 50 kHz, 150 kHz and 300 kHz. To this end, 175 circular cavities in a hexagonal arrangement, embedded in an infinitely extended cementitious matrix with the properties of Table 1, are considered. The representative volume element of this periodic structure corresponds to a void concentration of 10%. A longitudinal plane harmonic wave at the frequencies of 50 kHz, 150 kHz, 300 kHz and wavelengths 0.085 m, 0.0283 m, 0.0141 m, respectively, impinges upon the rows of cavities. The tractions fields created between the voids for the aforementioned frequencies are evaluated with the aid of the Boundary Element Method (BEM), which undoubtedly is the most accurate method for calculating stress fields in linear elastic structures. An advanced BEM, explained in [20, 21], is employed to this purpose. The traction fields, with respect to the propagation direction, are evaluated and shown in Fig. 13. Normalizing with the highest traction the results are presented, for each frequency, in a dimensionless scale from −1(compressive stress) to 1(tensile stress). Since the matrix is considered as a classical elastic material, it is apparent that high gradients of stresses correspond to high gradients of strains. As it can be seen from Fig. 13(a), qualitatively, there are certain areas where high stress and thus high strain gradients occur. These strain gradients appear as sudden changes of the contour colors from blue to cyan and red to yellow in the compressive and tensile regions, respectively. Mainly, they appear in the region between the voids and in a direction being perpendicular to the wave propagation. Similar results obtained in the recent work [22] where strain gradients appear in the body of bended perforated plates. Although the figure seems to be different in Fig. 13(b) and (c), a careful observation reveals that almost all the regions between the holes appear sudden changes from tensile to compressive tractions, which are associated with significant strain gradients. Such a behavior justifies the use of strain gradient elasticity as a theory that can capture dispersion phenomena in damaged concrete.

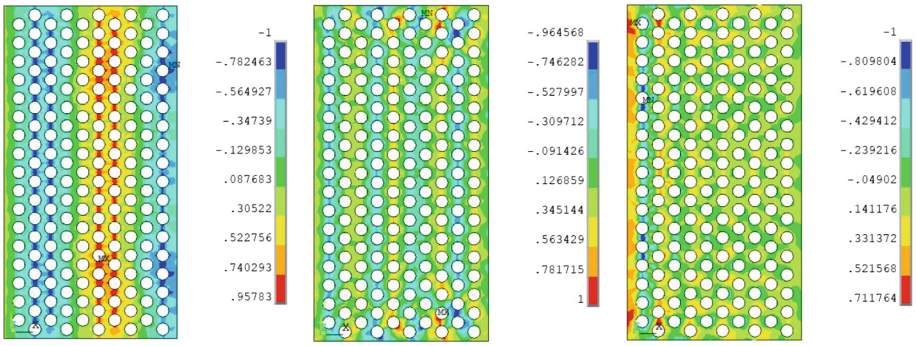

(a) (b) (c)

Fig. 13. Distribution of tractions along the direction of a longitudinal elastic wave propagating in a concrete matrix containing 10% hexagonally distributed circular voids. The propagating wave is harmonic at the frequencies of (a) 50 kHz, (b) 150 kHz and (c) 300 kHz.

6 Conclusions

The present numerical investigation sheds light into the effect of shape of inclusions (voids) in the wave propagation velocity in an elastic matrix. Results highlight the dispersive nature of the heterogeneous material. The pulse velocity increases with frequency between 50 and 500 kHz by as much as 12%, making frequency a very crucial parameter of any ultrasonic test in concrete. Furthermore, the differences between inclusion shapes are more evident at low frequencies where the wavelength is much longer than the heterogeneity size and tend to diminish for higher frequency where the wavelength is of the same order with the inclusion size. Results show that the circular shape of inclusion is a generally good approximation resulting however, in velocities a few percent higher than the average of the different shapes. Care should be taken when there is a specific orientation preference of heterogeneity. Then the wave direction relatively to the voids orientation becomes relevant and the result may differ by almost 30% between favorable and unfavorable direction. In addition, experimental results obtained by plate-like inclusions are presented showing strong similarity with the numerical cases concerning ellipsoidal vertical inclusions. Finally, the numerical results are compared with theoretical from scattering models and Mindin's gradient elastic theory, showing a convergence and implying that all different approaches are different prisms to study the same phenomenon.

References

1. Naik, T.R., Malhotra, V.M., Popovics, J.S.: The ultrasonic pulse velocity method. In: Malhotra, V.M., Carino, N.J. (eds.) Handbook on Nondestructive Testing of Concrete. CRC Press, Boca Raton (2004)

2. Anderson, D.A., Seals, R.K.: Pulse velocity as a predictor of 28-and 90-day strength. ACI J. **78–9**, 116–122 (1981)
3. Chaix, J.F., Garnier, V., Corneloup, G.: Ultrasonic wave propagation in heterogeneous solid media: theoretical analysis and experimental validation. Ultrasonics **44**(2), 200–210 (2006)
4. Punurai, W., Jarzynski, J., Qu, J., Kurtis, K.E., Jacobs, L.J.: Characterization of entrained air voids in cement paste with scattered ultrasound. NDT E Int. **39**(6), 514–524 (2006)
5. Iliopoulos, S.N., Aggelis, D.G., Polyzos, D.: Wave dispersion in fresh and hardened concrete through the prism of gradient elasticity. Int. J. Solid Struct. **78**, 149–159 (2016)
6. Waterman, P.C., Truell, R.: Multiple scattering of waves. J. Math. Phys. **2**, 512–537 (1964)
7. Mindlin, R.D.: Microstructure in linear elasticity. Arch. Rat. Mech. Anal. **16**, 51–78 (1964)
8. http://www.cyberlogic.org/wave2000.html. Accessed April 2019
9. Kaufman, J.J., Luo, G., Siffert, R.S.: Ultrasound simulation in bone. IEEE Trans. Ultrason. Ferroelectr. Freq. Control **55**(6), 1205–1218 (2008)
10. Philippidis, T.P., Aggelis, D.G.: Experimental study of wave dispersion and attenuation in concrete. Ultrasonics **43**(7), 584–595 (2005)
11. Aggelis, D.G., Shiotani, T.: Effect of inhomogeneity parameters on wave propagation in cementitious material. ACI Mater. J. **105**(2), 187–193 (2008)
12. Aggelis, D.G., Polyzos, D., Philippidis, T.P.: Wave dispersion and attenuation in fresh mortar: comparisons of theory with experimental measurements. J. Mech. Phys. Solids **53**, 857–883 (2005)
13. Villarreal, A., Solis-Najera, S., Medina-Gomez, L.: Application of Waterman-Truell and the dynamic generalized self-consistent models on concrete. Phys. Proc. **70**, 437–441 (2015)
14. Yu, T., Chaix, J.-F., Komatitsch, D., Garnier, V., Audibert, L., Henault, J.-M.: 2D numerical modeling of ultrasonic wave propagation in concrete: a parameterization study in a multiple-scattering medium. In: AIP Conference Proceedings, vol. 1806, p. 080011 (2017). https://doi.org/10.1063/1.4974636
15. Iliopoulos, S.N., Malm, F., Grosse, C.U., Aggelis, D.G., Polyzos, D.: Interpretation of concrete's microstructural coefficients through Mindlin's strain gradient elastic theory and controlled experiments. J. Acoust. Soc. Am. **142**(1), 89–94 (2016)
16. Dona, M., Lombardo, M., Barone, G.: Experimental study of wave propagation in heterogeneous materials. In: Kruis, J., Tsompanakis, J., Topping, B.H.V. (eds.) Proceedings of the Fifteenth International Conference on Civil, Structural and Environmental Engineering Computing, Prague, 1–4 September, Paper 208 (2015)
17. Hassanpour, S., Heppler, G.R.: Micropolar elasticity theory: a survey of linear isotropic equations, representative notations, and experimental investigations. Math. Mech. Solids 1–19 (2015). https://doi.org/10.1177/1081286515581183
18. Lewis, T.S., Kraft, D.W., Hom, N.: Scattering of elastic waves by cylindrical cavity in a solid. J. Appl. Phys. **47**(5), 1795–1798 (1976)
19. Aggelis, D.G., Tsinopoulos, S.V., Polyzos, D.: An iterative effective medium approximation (IEMA) for wave dispersion and attenuation predictions in particulate composites suspensions and emulsions. J. Acoust. Soc. Am. **116**(6), 3443–3452 (2004)
20. Polyzos, D., Tsinopoulos, S.V., Beskos, D.E.: Static and dynamic boundary element analysis in incompressible linear elasticity. Eur. J. Mech. A/Solids **17**(3), 515–536 (1998)
21. Gortsas, T.V., Tsinopoulos, S.V., Polyzos, D.: An advanced ACA/BEM for solving 2D large-scale problems with multi-connected domains. CMES: Comput. Model. Eng. Sci. **107** (4), 321–343 (2015)
22. Gortsas, T.V., Tsinopoulos, S.V., Rodopoulos, D., Polyzos, D.: Strain gradient elasticity and size effects in the bending of fiber composite plates. Int. J. Solids Struct. **143**, 103–112 (2018)